New Journal of Physics
The open access journal at the forefront of physics

Deutsche Physikalische Gesellschaft DPG IOP Institute of Physics

PAPER

Mechanism of non-classical light emission from acoustically populated (311)A GaAs quantum wires

New Journal of Physics
The open-access journal for physics

Mechanism of non-classical light emission from acoustically populated (311)A GaAs quantum wires

S Lazić[1], **R Hey and P V Santos**

Paul-Drude-Institut für Festkörperelektronik, Hausvogteiplatz 5-7,
10117 Berlin, Germany
E-mail: snezana@pdi-berlin.de

New Journal of Physics **14** (2012) 013005 (12pp)
Received 2 August 2011
Published 6 January 2012
Online at http://www.njp.org/
doi:10.1088/1367-2630/14/1/013005

Abstract. We employ surface acoustic waves (SAWs) to control the transfer of photo-generated carriers between interconnected quantum wells and quantum wires (QWRs) grown on pre-patterned (311)A GaAs substrates. Optical studies, carried out under remote acoustic excitation of a single QWR, have shown sharp photoluminescence lines and antibunched photons with tunable emission energy. These features are attributed to recombination of acoustically transported carriers in potential inhomogeneities within the wire. The origin of the photon antibunching is discussed in terms of a 'bottleneck' in the number of carriers trapped in the QWR, which restricts the number of recombination events per SAW cycle. We propose a model for antibunching based on the trapping of carriers induced by the SAW piezoelectric field in states at the interface between the GaAs QWR and the AlGaAs barriers. Non-classical light is emitted during the subsequent release of the trapped carriers into the recombination centers within the wire. The spatial distribution of the emitting recombination centers is estimated using time-resolved measurements.

[1] Author to whom any correspondence should be addressed.

Contents

1. Introduction

Single-photon sources (SPSs) play an important role in a variety of experiments in quantum optics and quantum information science, particularly in quantum key distribution, quantum teleportation and linear optics quantum computation [1, 2]. Various methods of obtaining single-photon emission have been investigated, including semiconductor systems. Due to their tailorable electronic and optical properties, low-dimensional semiconductor structures, such as quantum wires (QWRs) and quantum dots (QDs), have emerged as promising platforms for single-photon emitters [3, 4] and quantum logic elements [5, 6] in quantum information processing. Also, the fabrication of low-dimensional semiconductor structures is compatible with mature semiconductor technologies, allowing them to be integrated with other components on a single chip. However, the generation of single photons in a well-controlled manner and with high repetition rates in semiconductor heterostructures is still a challenge. Such sources of single photons operating 'on demand' at high repetition rates are desirable for quantum light applications.

One way of generating single photons at a high repetition rate is to employ a surface acoustic wave (SAW) propagating on a piezoelectric semiconductor (such as, for instance, GaAs) to produce a moving piezoelectric potential modulation, which can confine and transport electronic excitations over macroscopic distances. It has been shown that an SAW can be used to realize various functionalities relevant to quantum information devices, including carrier transport [7], single-electron pumps [8], light storage [9], spin transport and manipulations [10, 11] and photon detectors [12]. The idea of using SAWs in semiconductor systems to generate single photons on request was suggested by two groups [13–16]. The acoustically triggered SPS was first realized in InAs QD systems by employing an SAW to modulate the energy levels of single QDs [17].

Recently, we demonstrated the controlled emission of antibunched photons in (311)A (Al,Ga)As heterostructures grown on patterned substrates, by using an SAW to transfer carriers from a quantum well (QW) to the embedded QWRs [18]. The emission of antibunched photons was attributed to the recombination of acoustically transported holes with the electrons trapped in the potential inhomogeneities within the QWRs. The confining potential of these QD-like

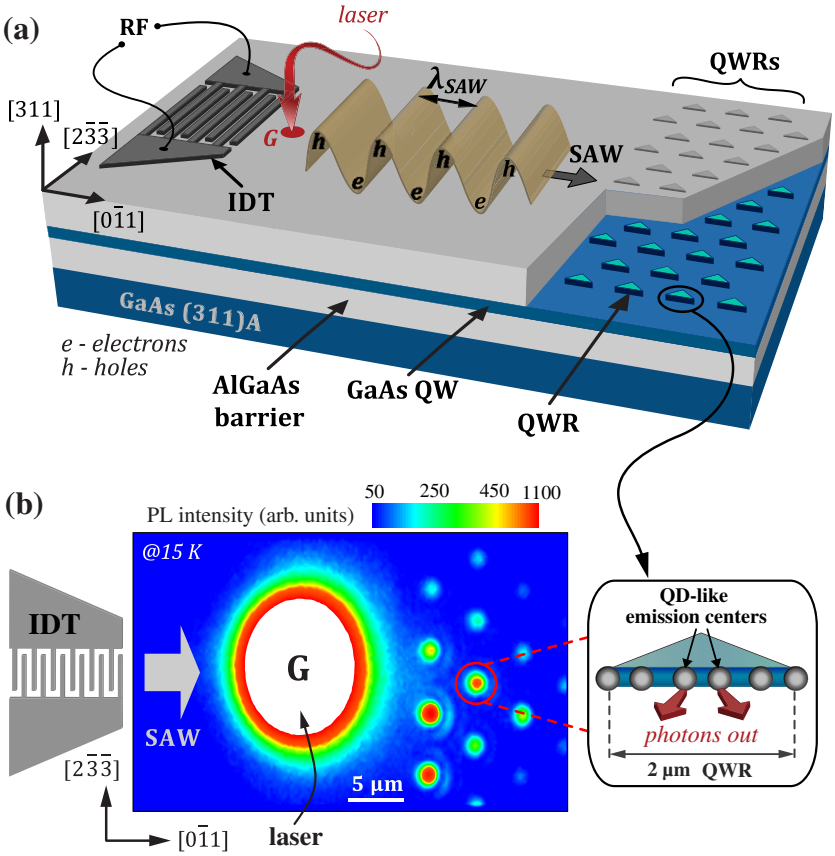

Figure 1. (a) The setup for an acoustically driven source of antibunched photons using a QWR coupled to a (311)A GaAs QW. The coupled structures are formed during the growth by molecular beam epitaxy on a (311)A GaAs substrate patterned with shallow triangular mesas. A controllable transport of electrons (e) and holes (h), optically excited in the QW at the generation point G, is achieved using an SAW. The SAW is generated by applying a radio-frequency (RF) signal to an interdigital transducer (IDT). Inset: photons are emitted when the transported carriers recombine in the discrete QD-like states within the QWR. (b) PL image of the acoustic transport: 2 μm long QWRs (sketched in the inset) appear as bright luminescence spots along the SAW propagation path.

recombination centers was found to be of the order of 2–3 meV and was ascribed to the monolayer thickness fluctuations on the (311)A QWR facet. The experiments reported in [18] (also illustrated in figure 1(a)) have shown that the SAW-driving mechanism can be used to tune the energy of the emitted photons by selectively populating a particular emission center within the QWR. This behavior was seen in a number of QWRs within the sample, thus indicating that the observed phenomenon is a characteristic property of our system. The experiments have also demonstrated that SAW pumping reduces the timing jitter for the emission of antibunched photons, thus facilitating the realization of SPS operating at several hundreds of MHz. Such a high repetition rate of the single photons is similar to that available from InAs QDs [17, 19], but it can be further increased by using higher SAW frequencies.

In this paper, we investigate the mechanisms leading to the non-classical light emission from the acoustically excited QWRs. From the measured photon statistics, we observe that the quantitative estimate for the temporal correlation between emitted photons is independent of the remote excitation conditions (namely the applied acoustic intensity and laser excitation density). We attribute the origin of the non-classical light emission to a 'bottleneck' effect, which restricts the number of carriers trapped at the QWR close to the recombination sites and hence prevents simultaneous emission from multiple recombination centers. To explain this effect, we propose a physical model based on piezoelectrically assisted injection of electrons into non-radiative interface states during one SAW half-cycle, and their release into the QWR in a subsequent half-cycle, where they recombine with transported holes. In this way, the antibunching of the emitted photons is dictated by a fixed number of carriers trapped at interface states, whereas the energy of the photons is determined by the SAW-governed selection of the recombination centers within the QWR. Moreover, the spatial distribution of these recombination centers, which could not be determined from spatially resolved photoluminescence (PL) experiments, is estimated from time-resolved PL (TRPL) spectroscopy combined with ambipolar acoustic transport.

This paper is organized as follows. We first give in section 2 a brief description of the sample fabrication and experimental techniques. In section 3, we discuss our experimental results and construct a consistent physical model to account for all experimental observations. Concluding remarks are given in section 4.

2. Experimental details

2.1. Sample fabrication

The (Al,Ga)As layers in the sample were deposited via molecular beam epitaxy on (311)A GaAs substrate, patterned with shallow (35 nm high) triangular mesas (cf figure 1(a)). The mesas were produced using conventional photolithography techniques and selective wet chemical etching. Details of the fabrication process are given elsewhere [20–22].

The overgrown layers consist of a nominally 6 nm thick GaAs QW surrounded by 150 nm $Al_{0.33}Ga_{0.67}As$ barriers and capped with a 20 nm thick GaAs layer. Approximately 50 nm wide and 12 nm high QWRs form during growth due to (i) preferential attachment of the material at mesa sidewalls aligned along the $[0\bar{1}1]$ direction [23] and (ii) the compositional disproportionation of the (Al,Ga)As barriers induced by facet-dependent variation of the local Al concentration [24]. The latter is attributed to the inhomogeneous incorporation of Ga adatoms due to the anisotropy of the migration length and its dependence on surface orientation [24]. In addition, potential inhomogeneities along the wire axis, which are due to fluctuations in the QWR thickness and in the barrier composition, may act as carrier traps and induce recombination. As a result, the sidewall QWRs consist of a sequence of QD-like emission centers, illustrated in the inset of figure 1 [23, 25].

2.2. Experimental setup

The SPS is realized using an SAW to transfer carriers, which are optically generated in the QW at the position G (cf figure 1(a)), to the QWRs. SAWs propagating in the QW plane along the $x = [0\bar{1}1]$ direction are excited by applying an RF signal to an IDT deposited on

the sample surface. The IDT operates at a wavelength of $\lambda_{SAW} = 4\,\mu$m, which is established by the interdigital electrode spacing and corresponds to a frequency $f_{SAW} = 751$ MHz.

The carrier transfer takes place through the ionization of the photoexcited electron–hole (e–h) pairs by the SAW piezoelectric field [9]. The carriers are then spatially separated into electron and hole charge packets (cf figure 1(a)) and transported at the well-defined sound velocity $v_{SAW} = f_{SAW}\lambda_{SAW}$ towards the QWRs, where they recombine radiatively. The optical studies were carried out by low-temperature ($\sim$15 K) PL microscopy. In the experiments, short laser pulses (approximately 90 ps pulse width) emitted at 635 nm were focused onto the SAW path using a 50$\times$ microscope objective. The laser repetition rate was synchronized with the RF generator employed to drive the IDT. The PL from the sample was collected by the same objective and imaged onto a 100 micron pinhole to select the emission from a single QWR. The signal is then spectrally dispersed and imaged by a 640 mm focal length monochromator (T64000 Horiba Jobin Yvon) equipped with a nitrogen-cooled charge coupled device (CCD) camera or fed to a Hanbury-Brown and Twiss (HBT) setup for TRPL or photon correlation experiments. Optical filtering was used to remove the stray light from the laser as well as the emission originating from the QW. The HBT setup consists of two photodetectors (PerkinElmer, SPCM-AQRH-14 and 15) placed in one of the two output ports of a 50/50 non-polarizing beam-splitter and connected to the either 'start' or 'stop' inputs of a time-correlated single-photon counting electronics (Picoquant Picoharp 300). The experiment delivers a histogram showing the temporal distribution of the coincidences of two photodetectors. For time-resolved measurements, the time delay measuring electronics was started on a signal derived from the pulsed excitation and stopped on detection of a photon.

3. Results and discussion

3.1. Remote photoluminescence: spectroscopic studies

The recombination of the carriers acoustically transported in the QW plane and captured by the confinement potential of the QWRs leads to the PL micrograph illustrated in figure 1(b). Spectral analysis of the light emitted from a single QWR is depicted in figure 2. The sharp PL lines (upper panels of figure 2), which are observed over a wide range of acoustic powers (specified in terms of the electrical powers P_{rf} applied to the IDT), are attributed to the recombination of the transported holes with the electrons trapped in the QWR during a previous SAW cycle [18]. As shown in the PL spectra of figure 2, the recombination probability, and hence the spectral shape of the PL, changes with the intensity of the SAW, as the SAW piezoelectric field becomes strong enough to overcome the barriers imposed by potential fluctuations within the QWR. Thus, the selection of recombination centers in the QWR relies on the fact that the SAW not only injects but also extracts carriers from them. For low P_{rf} values, the transported holes recombine with a high density of electrons trapped in the QWR, leading to the large number of lines spread over a range of approximately 10 meV (cf the PL spectrum for $P_{rf} = -6$ dBm in the upper panel of figure 2(a)). In contrast, for high acoustic powers ($P_{rf} = 10$, 13 and 16 dBm), the density of trapped electrons reduces and fewer recombination events are detected. It therefore becomes possible to selectively populate a single emission center within the QWR simply by tuning the SAW power, which gives rise to a single-photon emission.

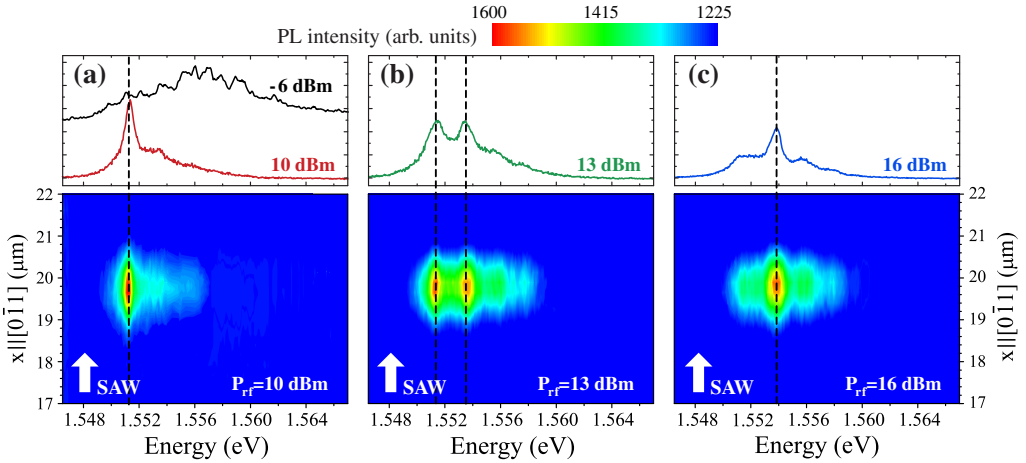

Figure 2. Lower panels: time-integrated PL intensity plotted as a color scale versus emission energy (horizontal axis) and distance from the illumination spot (vertical axis). The light was collected from a single QWR marked in figure 1. The selected QWR is aligned along the SAW propagation direction $x = [0\bar{1}1]$ and remotely excited under SAWs with (a) $P_{rf} = 10$ dBm, (b) $P_{rf} = 13$ dBm and (c) $P_{rf} = 16$ dBm. The dashed vertical lines mark the spectral position of the two emission centers within the QWR. Upper panels: the corresponding PL spectra for $P_{rf} = -6$, 10, 13 and 16 dBm.

3.2. Time-resolved photoluminescence

The spatial extension of the localized emission centers in figure 2 is below the spatial resolution of our optical system, thus making it difficult to determine their precise location. In order to extract information concerning their spatial distribution, we display in figure 3 the temporal dependence of the PL emitted from the selected QWR at different P_{rf} values. The excitation time was established by measuring the reflectance of the pulsed laser excitation (trace labeled 'laser'). In the absence of an SAW (trace labeled 'no SAW'), only the luminescence close to $t = 0$ is observed due to imperfect filtering of the QW emission from the excitation spot. When an SAW is applied, the remotely detected PL signal at the QWR position consists of a series of pulses separated by the SAW period $T_{SAW} = 1.33$ ns.

The repetition rate of these oscillations indicates that both carrier transport and recombination take place synchronously with the SAW frequency ($f_{SAW} = 1/T_{SAW} = 751$ MHz). This is confirmed by the delayed arrival of the PL onset relative to the excitation pulse (of approximately 6 ns), which corresponds to the time needed to transport the carriers from the excitation spot (G in figure 1) to the selected QWR at well-defined SAW velocity v_{SAW}. By taking into account that the carriers are transported with v_{SAW}, the average separation between the two emission centers of figure 2 can be obtained from the time shift between the PL pulses emitted from each emission center, which are selectively populated using $P_{rf} = 10$ and 16 dBm, respectively. The observed maximum time shift of $\Delta t = 70$ ps (cf the inset in figure 3) yields an upper limit for the spatial separation $\ell_{max} = v_{SAW}\Delta t$ between the emission centers of approximately 210 nm. This value compares well with the average spatial extension of the emission regions of about 150 nm, which was obtained from near-field PL studies carried out

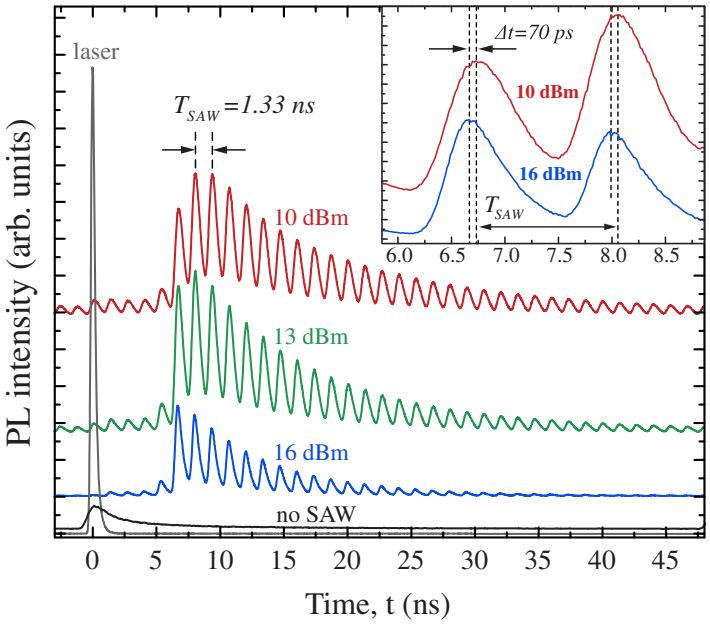

Figure 3. Temporal profile of the excitation pulse (trace labeled 'laser') and the PL emitted from QWR of figure 2 under acoustic excitation ($P_{rf} = 10$, 13 and 16 dBm) and in the absence of SAW (curve labeled 'no SAW'). The traces are vertically shifted for clarity. The inset shows an enlarged portion (from $t = 5.85$ to 8.85 ns) of the decay profiles recorded using $P_{rf} = 10$ and 16 dBm.

on similar structures [26]. Note that the photon emission region is much smaller than the total length of the QWR, which is of the order of half of the acoustic wavelength ($\lambda_{SAW}/2 = 2\,\mu$m). Under these conditions, the acoustic transport reduces the time available for recombination to values below $T_{SAW}/2$. The short recombination times result from the fact that the time window during which the spatial location of the transported holes overlaps with the electron trapping site is much shorter than $T_{SAW}/2$. Consequently, the amplitudes of the PL pulses in figure 3 are limited by the temporal response of the detector (~400 ps), rather than by the carrier recombination times. Such fast recombination dynamics reduces the jitter in the photon emission time, therefore allowing for high photon repetition rates.

3.3. Non-classical light emission: photon correlation measurements

The statistics of the photons emitted from the remotely excited QWR was analyzed using the HBT setup described previously. The measurements depicted in figure 4(a) (three upper histograms) display a number of correlation peaks separated by the SAW period T_{SAW}. These well-defined short-period oscillations arise from the periodic modulation of the photon emission probability by the SAW. The longer periodicity is due to the laser repetition rate, which is evident in the lowest histogram in figure 4(a) recorded in the absence of an SAW for local excitation directly on the QWR. A clear reduction of the coincidence rate at zero-time delay (photon antibunching) is observed under remote acoustic excitation. These antibunching minima reflect the reduced probability for simultaneous emission of multiple photons, thereby proving the non-classical character of the emitted light.

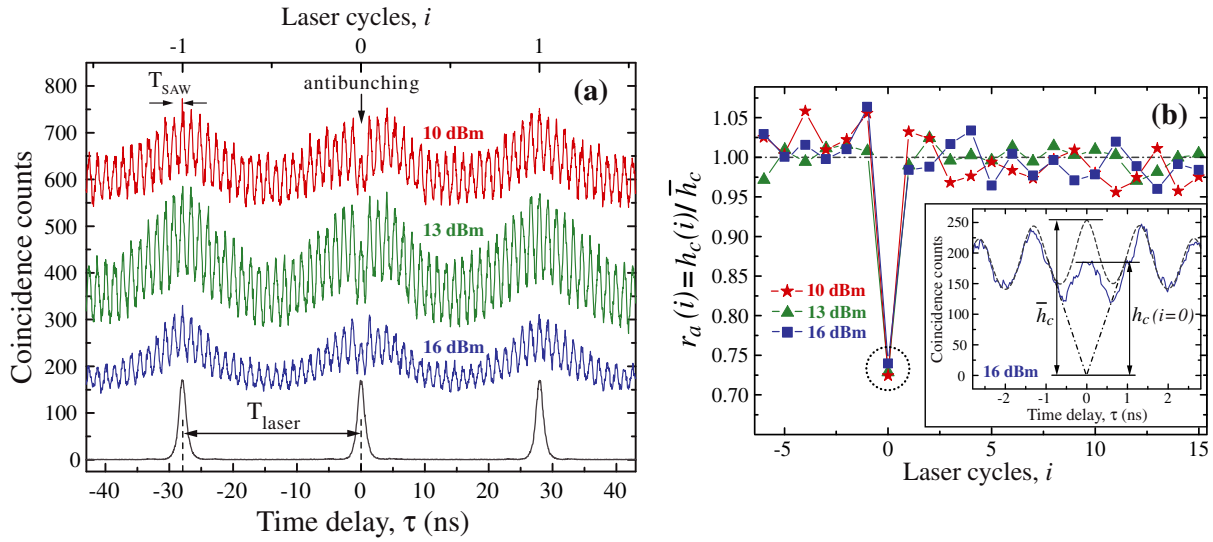

Figure 4. (a) Photon correlation histograms for the QWR in figures 2 and 3 recorded under the same remote excitation conditions ($P_{\mathrm{rf}} = 10$, 13 and 16 dBm). The traces are vertically offset for clarity. The short and long oscillations correspond to correlation events with the periodicity of the SAW ($T_{\mathrm{SAW}} = 1.33$ ns) and the laser pulses ($T_{\mathrm{laser}} = 27.94$ ns). The lower histogram is measured on the same QWR for direct optical excitation and in the absence of SAW. (b) Normalized intensities of the central coincidence peaks $h_{\mathrm{c}}(i)$ for laser cycles $i = -6, -5, \ldots, 33$. Symbols at $\tau = 0$ surrounded by a dotted circle represent the degree of antibunching for $P_{\mathrm{rf}} = 10$ dBm (star), 13 dBm (triangle) and 16 dBm (square). Inset: magnified portion of the 16 dBm HBT histogram of figure 4(a). The dashed envelope reflects the average intensity $\overline{h}_{\mathrm{c}}$ of $h_{\mathrm{c}}(i \neq 0)$ peaks. The dot-dashed lines represent the overlap of the neighboring side peaks, which determines the resolution-limited background level.

It is interesting to note that the antibunching dip at $\tau = 0$ is observed for different P_{rf} values, which lead to different photon emission energies in figures 2(a)–(c). Thus, in the SPS presented here, the energy of the emitted photons can be tuned by controlling the SAW power. Also, no significant broadening of the $\tau = 0$ coincidence peak has been observed for all histograms in figure 4(a), therefore confirming the narrow spatial distribution of the emission centers revealed by the TRPL analysis discussed above.

As for the TRPL results in figure 3, the visibility of the coincidence peaks in the HBT histograms is affected by the finite time resolution of our HBT setup. In order to quantify the degree of antibunching, the amplitude of the central coincidence peaks at $\tau = i\,T_{\mathrm{laser}}$ (denoted by $h_{\mathrm{c}}(i)$ for the ith laser cycle) has to be measured relative to the background level induced by the resolution-limited overlap with adjacent side peaks. For that purpose, we use the extrapolation process indicated by the dot-dashed lines in the inset of figure 4(b).

In analogy to the quantum emitters probed by pulsed laser excitation, we define the degree of antibunching as $r_{\mathrm{a}}(i = 0) = h_{\mathrm{c}}(i = 0)/\overline{h}_{\mathrm{c}}$, where $\overline{h}_{\mathrm{c}}$ represents the count rate averaged over all central peaks $h_{\mathrm{c}}(i)$ with $i \neq 0$.[2] $\overline{h}_{\mathrm{c}}$ can also be obtained by the auto-correlation of time-resolved

[2] The histograms were recorded for delays τ covering up to 40 laser cycles.

traces (cf figure 3) recorded under identical conditions—one example is indicated by the dashed envelope in the inset of figure 4(b). The ratio $r_a(i = 0)$ can be used as a parameter to monitor deviations from a classical light source. For all photon correlation histograms in figure 4(a), this ratio falls in the range of 70–75%. For comparison, we display in figure 4(b) the ratio $r_a(i)$ for all laser cycles i. We find with more than 99.7% confidence that $r_a(i) = 1 \pm 0.025$ for $i \neq 0$. The $r_a(i = 0)$ values (marked by a dotted circle in figure 4(b)), which are indicative of antibunching, are lower than those for $i \neq 0$ by at least eight standard deviations, thus clearly proving the quantum nature of the phenomenon.

The $r_a(i = 0)$ values in the range 70–75% imply that the probability of detecting multiple photons is reduced by approximately 25–30% in comparison to a coherent source of the same intensity. If N photons impinge on a beam-splitter of the HBT setup at the same time, the coincidence count at $\tau = 0$ will not vanish completely but drop to a value of $r_a(i = 0) = 1 - 1/N$ [27]. The non-zero coincidence rate at $\tau = 0$ then suggests that, on average, fewer than four ($N < 4$) photons are emitted from the QWR per SAW cycle. Interestingly, the degree of antibunching and hence, the number of emitted photons, does not change significantly with P_{rf} (cf figure 4(b)).

To explain these observations, we invoke two possible mechanisms that could lead to the on-demand emission of antibunched photons from such acoustically driven semiconductor systems. In the first, the number of recombination events, and therefore the number of emitted photons, is limited by the number of carriers transported per SAW cycle [13]. Namely, if only a few carriers (<4) are transported per T_{SAW}, their recombination at the selected QWR could lead to the observed levels of antibunching. The second mechanism assumes that the number of recombination events is limited by some kind of 'bottleneck' in the carrier recombination at the QWR, so that only a few centers (<4) within the QWR can emit at the same time.

To investigate the relative contribution of these two mechanisms, we plot in figure 5(a) the degree of antibunching as a function of the laser excitation power P_{exc} at constant SAW power. The constant P_{rf} value ensures that the efficiency of the acoustic transport as well as the carrier capture into and extraction from the QD-like states within the QWR does not vary with P_{exc}. P_{exc} controls the number of photoexcited carriers and hence the average number (n) of carriers transported to the selected QWR per SAW cycle. n was determined by measuring the quenching levels of the PL emitted from the illumination area under the applied SAW. As shown in figure 5(a), the degree of antibunching remains practically unchanged with increasing the number of transported carriers. This result suggests that the non-classical light emission is governed by the 'bottleneck' in the carrier recombination within the QWR (corresponding to the second mechanism), rather than by the number of transported carriers (the first mechanism). Also, the emitted photons must originate from the first lowest excited state since, with increasing the laser excitation power, the contribution from the higher excited states would increase the probability of multi-photon emission and hence reduce the antibunching.

3.4. Non-classical light emission: model

The origin of the invoked recombination 'bottleneck' might be discussed in terms of Coulomb-mediated capture processes, which control the population of the emission centers within the QWR. In analogy to the Coulomb blockade within a single QD [28], the repulsion between the trapped charges reduces the probability of trapping multiple electrons within the QWR, thereby reducing the number of recombination events and hence the number of photons emitted per

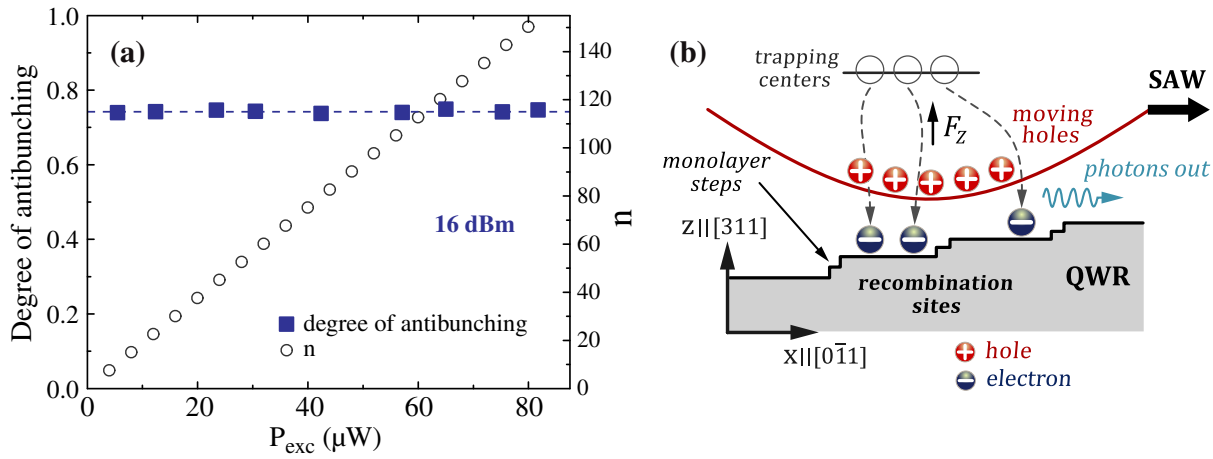

Figure 5. (a) Dependence on the laser excitation power P_{exc}: (left axis) the degree of antibunching and (right axis) the average number (n) of transported carriers reaching the QWR per $T_{SAW}/2$. The latter was calculated by using the relative changes in the integrated PL intensities as a measure of the carrier densities. (b) Schematic illustration of the mechanism responsible for the non-classical light emission from acoustically excited QWR: the vertical arrow labeled F_z shows the orientation of the transverse components of the SAW piezoelectric field during the passage of a hole packet. The empty cycles represent the non-radiative electron traps at the interface (indicated by a flat horizontal line) with the upper $Al_{0.33}Ga_{0.67}As$ barrier. The carrier recombination sites within the QWR are represented by the stepped horizontal line showing the non-planar surface configuration of the QWR.

SAW cycle. Although the above model can explain the magnitude of the antibunching effect in figure 4(b) and its insensitivity to the excitation conditions (determined by P_{exc} and P_{rf}), it cannot account for the changes in spectral shape and in the number of lines in the time-integrated PL spectra recorded at different P_{rf} values (cf the upper panels in figures 2(a)–(c)).

To account for all of the experimental results, we now propose the alternative model schematically sketched in figure 5(b). This model is based on the capture of electrons into non-radiative trapping sites close to the upper interface with the $Al_{0.33}Ga_{0.67}As$ barrier. It also assumes that there are regions in the QWR with different band gaps, induced by fluctuations in layer thickness and in the composition of the barriers, which act as carrier recombination sites. Hence, in the proposed model, the electron trapping centers do not correspond to the recombination sites. Trapping of electrons is assisted by the transverse component F_z (i.e. along the growth direction as indicated by a vertical arrow in figure 5(b)) of the SAW piezoelectric field. For the P_{rf} values in figures 3 and 4, F_z becomes strong enough to squeeze the electron and hole wave functions towards the upper interface [29]. Due to their lower mass, the electrons are more susceptible to such a mechanism, yielding more efficient transfer of electrons from an electron packet into interface traps. During the passage of holes in a subsequent SAW half-cycle, the direction of F_z reverses and thus assists in the release of trapped electrons into the QWR. These electrons, being exposed to an abundance of holes, then recombine radiatively within the QWR as illustrated in figure 5(b). The number of recombination events is therefore

determined by the number of electrons trapped at non-radiative interface states. This number should depend weakly on P_{rf} and P_{exc}, which is in agreement with the experimental results depicted in figures 4(b) and 5(a). For a low density of interface traps, only a few recombination events per SAW cycle will occur, thus leading to the observed levels of antibunching (cf figure 4(b)). Assuming an interface state density of the order of 10^{10}–10^{11} cm^{-2} (typically observed for high-quality AlGaAs/GaAs (001) hetero-interfaces [30]), we estimate the presence of approximately 1–10 interface traps within the 200 nm long emission region of the 50 nm wide QWR, which is consistent with our results ($N < 4$). In contrast, the recombination probability within the QWR depends on the acoustic intensity (see section 3.1), which triggers the redistribution of electrons between different recombination centers during the photon emission cycle $T_{SAW}/2$. Consequently, for a fixed number of interface states, the emission spectra can change with P_{rf} while maintaining the same degree of antibunching, as observed in the experiments of figures 2(a)–(c) (upper panels) and figure 4(b), respectively.

The origin of interface traps is still unclear. They could be associated with inherent structural inhomogeneities arising from, e.g., interface roughness, compositional non-uniformity or lattice imperfections. However, their low density and predominant electron-trapping character indicate that other sources of selective electrons traps, such as charge impurities, may also be considered.

4. Conclusions

We have demonstrated that an SAW can be used to generate antibunched photon pulses on demand from QWRs coupled to (311)A GaAs QWs. The antibunched photons are emitted at a high repetition rate when the acoustically transported carriers recombine in the potential inhomogeneities within the QWRs. We show that by changing the acoustic intensity we can tune the energy of the emitted photons by selectively populating different emission centers within the QWR. The TRPL spectroscopy was employed to obtain information regarding the spatial distribution of otherwise spatially unresolved emission centers. This method can be useful in effectively adding spatial resolution to conventional optical microscopy without resorting to high-spatial-resolution techniques such as scanning near-field optical microscopy.

The photon correlation measurements demonstrate the feasibility of SAW-driven on-demand SPSs. The measurements yield a quantitative estimate of the correlation between emitted photons (25–30% compared to a coherent source of the same intensity), thus proving the non-classical nature of the source. The origin of the non-classical light emission was discussed in terms of field-assisted capture of electrons by non-radiative interface states close to the upper $Al_{0.33}Ga_{0.67}As$ barrier. The trapped electrons are released during a subsequent SAW half-cycle into the QWR, where they recombine with holes. Our results indicate that the degree of antibunching is dictated by a fixed number of interface states, whereas the energy of the emitted single photons is determined by the SAW-governed selection of the recombination sites within the QWR.

The observed levels of antibunching suggest a low density of interface traps. Further investigations are necessary to clarify the microscopic origin of these traps. Also, considerable improvements in the antibunching levels and in the photon throughput are required for applications in SPSs. The latter can be achieved by embedding the QWRs in an optical microcavity to enhance light extraction efficiency. The degree of antibunching can be enhanced by reducing the density of interface traps. This can be achieved through optimization of the

growth conditions or by using shorter QWRs. These procedures will not only improve the photon source but also allow the verification of the mechanisms for non-classical light emission proposed in this paper.

Acknowledgment

We acknowledge W Seidel, E Wiebicke and M Höricke for help in the fabrication of the samples.

References

[1] Lounis B and Orritet M 2005 *Rep. Prog. Phys.* **68** 1129
[2] Yamamoto Y, Santori C, Solomon G, Vuckovic J, Fattal D, Waks E and Diamanti E 2005 *Prog. Inf.* **1** 5
[3] Michler P, Kiraz A, Becher C, Schoenfeld W V, Petroff P M, Zhang L, Hu E and Imamoglu A 2000 *Science* **290** 2282
[4] Santori C, Pelton M, Solomon S, Dale Y and Yamamoto Y 2001 *Phys. Rev. Lett.* **86** 1502
[5] Chen P, Piermarocchi C and Sham L J 2001 *Phys. Rev. Lett.* **87** 067401
[6] Craig N J, Taylor J M, Lester E A, Marcus C M, Hanson M P and Gossard A C 2004 *Science* **304** 565
[7] Hoskins M J, Morkoç H and Hunsinger B J 1982 *Appl. Phys. Lett.* **41** 332
[8] Shilton J M, Talyanskii V I, Pepper M, Ritchie D A, Frost J E F, Ford C J B, Smith C G and Jones G A C 1996 *J. Phys.: Condens. Matter* **8** L531
[9] Rocke C, Zimmermann S, Wixforth A, Kotthaus J P, Böhm G and Weimann G 1997 *Phys. Rev. Lett.* **78** 4099
[10] Stotz J A H, Hey R, Santos P V and Ploog K H 2005 *Nat. Matter* **4** 585
[11] Couto O D D, Iikawa F, Rudolph J, Hey R and Santos P V 2007 *Phys. Rev. Lett.* **98** 036603
[12] Jiao S J, Batista P D, Biermann K, Hey R and Santos P V 2009 *J. Appl. Phys.* **106** 053708
[13] Foden C L, Talyanskii V I, Milburn G J, Leadbeater M L and Pepper M 2000 *Phys. Rev.* A **62** 011803
[14] Hosey T, Talyanskii V, Vijendran S, Jones G A C, Ward M B, Unitt D C, Norman C E and Shields A J 2004 *Appl. Phys. Lett.* **85** 491
[15] Wiele C, Haake F, Rocke C and Wixforth A 1998 *Phys. Rev.* A **58** R2680
[16] Bödefeld C, Ebbecke J, Toivonen J, Sopanen M, Lipsanen H and Wixforth A 2006 *Phys. Rev.* B **74** 035497
[17] Gell J R, Ward M B, Young R J, Stevenson R M, Atkinson P, Anderson D, Jones G A C, Ritchie D A and Shields A J 2008 *Appl. Phys. Lett.* **93** 081115
[18] Couto O D D, Lazić S, Iikawa F, Stotz J A H, Jahn U, Hey R and Santos P V 2009 *Nat. Photonics* **3** 645
[19] Bennett A J, Unitt D C, See P, Shields A J, Atkinson P, Cooper K and Ritchie D A 2005 *Phys. Rev.* B **72** 033316
[20] Nötzel R, Temmyo J and Tamamura T 1994 *Appl. Phys. Lett.* **64** 3557
[21] Fricke J, Nötzel R, Jahn U, Niu Z C, Schönherr H-P, Ramsteiner M and Ploog K H 1999 *J. Appl. Phys.* **86** 2896
[22] Nötzel R and Ploog K H 2000 *Appl. Surf. Sci.* **166** 406
[23] Hey R, Friedland K J, Kostial H and Ploog K H 2004 *Physica* E **21** 737
[24] Limmer W, Bitzer K and Sauer R 2004 *Physica* E **23** 455
[25] Wang X-L and Voliotis V 2006 *J. Appl. Phys.* **99** 121301
[26] Intonti F, Emiliani V, Lienau C, Elsaesser T, Nötzel R and Ploog K H 2001 *Phys. Rev.* B **63** 075313
[27] Fox M 2006 *Quantum Optics: An Introduction* (New York: Oxford University Press) pp 156–63
[28] Livermore C, Crouch C H, Westervelt R M, Campman K L and Gossard A C 1996 *Science* **274** 1332
[29] Alsina F, Stotz J A H, Hey R and Santos P V 2006 *J. Vac. Sci. Technol.* B **24** 2029
[30] Krispin P, Hey R, Kostial H and Ploog K H 1997 *J. Appl. Phys.* **83** 1496